INSTITUTE OF PHYSICS PUBLISHING NANOTECHNOLOGY
Nanotechnology **17** (2006) S246–S252 doi:10.1088/0957-4484/17/11/S04

Comparison of laser-ablation and hot-wall chemical vapour deposition techniques for nanowire fabrication

E Stern[1,6], G Cheng[2,6], S Guthrie[3,6], D Turner-Evans[2], E Broomfield[2], B Lei[4], C Li[4], D Zhang[4], C Zhou[4] and M A Reed[2,5]

[1] Department of Biomedical Engineering, PO Box 208284, New Haven, CT 06520, USA
[2] Department of Electrical Engineering, PO Box 208284, New Haven, CT 06520, USA
[3] Department of Physics, PO Box 208284, New Haven, CT 06520, USA
[4] Department of Electrical Engineering-Electrophysics, University of Southern California, 3737 Watts Way, Los Angeles, CA 90089, USA
[5] Department of Applied Physics, PO Box 208284, New Haven, CT 06520, USA

E-mail: Eric.Stern@Yale.edu, Guosheng.Cheng@Yale.edu and Stan.Guthrie@Yale.edu

Received 5 January 2006, in final form 17 March 2006
Published 19 May 2006
Online at stacks.iop.org/Nano/17/S246

Abstract
A comparison of the transport properties of populations of single-crystal, In_2O_3 nanowires (NWs) grown by unassisted hot-wall chemical vapour deposition (CVD) versus NWs grown by laser-ablation-assisted chemical vapour deposition (LA-CVD) is presented. For nominally identical growth conditions across the two systems, NWs fabricated at 850 °C with laser-ablation had significantly higher average mobilities at the 99.9% confidence level, 53.3 ± 5.8 cm^2 V^{-1} s^{-1} versus 10.2 ± 1.9 cm^2 V^{-1} s^{-1}. It is also observed that increasing growth temperature decreases mobility for LA-CVD NWs. Transmission electron microscopy studies of CVD-fabricated samples indicate the presence of an amorphous In_2O_3 region surrounding the single-crystal core. Further, low-temperature measurements verify the presence of ionized impurity scattering in low-mobility CVD-grown NWs.

1. Introduction

Single-crystal, semiconducting nanowires (NWs) are a subject of intense contemporary interest because they represent the limit of crystalline semiconducting solids and have been successfully synthesized from a vast array of traditional semiconducting materials [1–12]. A number of growth techniques have been successfully implemented for NW synthesis including hot-wall chemical vapour deposition (CVD) [9] and laser-ablation-assisted hot-wall CVD (LA-CVD) [12]. Both fabrication methods are suggested to rely on the vapour–liquid–solid (VLS) mechanism, whereby gaseous vapour dissolves in a molten metal catalyst and then crystallizes into an NW, with nucleation at the substrate [9, 13]. However, the methods have been seen to produce NWs with significantly different transport properties: the mobilities of LA-CVD-fabricated NWs have been reported to be significantly greater than that of their CVD-grown counterparts [9, 14–16].

Here we present the first direct comparison to our knowledge of the electrical properties of an NW fabrication with LA-CVD and CVD in furnaces with similar growth conditions, in order to ascertain whether the NW quality was truly dictated solely by the source method. The NWs were characterized by fabrication into field effect transistors (FETs) utilizing a high-throughput approach [17] that produces statistically significant sample populations. Indium oxide NWs were chosen for the study because In_2O_3 NWs fabricated by laser-ablation in previous studies have been shown to reproducibly have good transport properties, with mobilities $\sim$111 cm^2 V^{-1} s^{-1} [12, 18–20]. Furthermore, these NWs

[6] These authors contributed equally to this work. Authors to whom any correspondence should be addressed.

Table 1. Material synthesis variables used for and device results from the LA and HW-CVD In_2O_3 NW study.

Growth	LA-CVD #1	LA-CVD #2	CVD #1[a]	CVD #2
Indium source material	InAs	InAs	InAs	InAs
Growth substrate	Si/SiO_2	Si/SiO_2	Si/SiO_2	Si/SiO_2
Pressure (Torr)	220	220	220	220
Metal catalyst	Au	Au	Au	Au
Oxygen flow rate	0.02% in 150 sccm Ar	0.02% in 150 sccm Ar	0.02% in 100 sccm Ar	0.02% in 100 sccm Ar
Substrate temperature (°C)	770	850	770	850
Source temperature (°C)	850	850	870	865
Mean diameter $\pm\sigma_M$ (nm)	32.5 ± 1.1	45.9 ± 3.6	47.5 ± 14.4[a]	50.6 ± 2.8
Mean mobility $\pm\sigma_M$ ($cm^2\ V^{-1}\ s^{-1}$)	111.8 ± 8.1	53.3 ± 5.8	25.1 ± 17.8[a]	10.2 ± 1.9
Mean carrier concentration $\pm\sigma_M$ (cm^{-3})	$1.3 \pm 1.2 \times 10^{18}$	$6.4 \pm 1.1 \times 10^{18}$	$3.1 \pm 1.6 \times 10^{19}$[a]	$4.8 \pm 2.2 \times 10^{18}$

[a] Note that samples from CVD #1 do not constitute a statistical sample and, as such, the error reported is the standard deviation, not the standard error of the mean.

are of particular interest because they have been successfully implemented as chemical and biochemical sensors [21–25].

2. Methods

The In_2O_3 NWs used for this study were synthesized either by LA-CVD or CVD, and the growth variables are tabulated in table 1. Though the growth furnaces were different, the setup was similar and all variables were held constant for each run. Nanowires were fabricated by LA-CVD at 770 °C (LA-CVD #1) because this growth temperature had previously been reported to be optimal [12]. However, we found that the NW yield for CVD-grown samples is strongly temperature-dependent and growths at 770 °C (CVD #1) produced very few NWs and thus few electronic devices could be fabricated. At 850 °C a high yield of NWs was obtained for both methods (LA-CVD #2 and CVD #2), which allowed for a statistically significant direct comparison.

In the LA-CVD approach, an InAs target is ablated with a pulsed laser to provide the necessary indium flux to a Si/SiO_2 substrate containing dispersed ∼30 nm Au clusters in a tube furnace with oxygen flowing, as previously described [12, 18]. In the CVD approach, a Si/SiO_2 substrate is coated with 3 nm of Au by electron-beam (e-beam) evaporation and placed in the tube furnace, a three-zone Mellen furnace, slightly downstream of the InAs source. The furnace is then rapidly heated and a constant oxygen flow is maintained; upon reaching the desired growth temperature, this temperature is maintained for 30 min, after which the system is radiantly cooled to ambient temperature. The yield was found to be critically dependent on the source–substrate distance, with an ideal separation of 5–15 mm.

Nanowires grown by LA-CVD and CVD were fabricated into electrical devices in parallel by optical lithographic processing [17]. The NWs were randomly dispersed on degenerately doped Si wafers with a 200 nm thermal oxide, which had previously been patterned and etched to define backside contacts. A resist bilayer was then applied, patterned, and subjected to an oxygen plasma, and a liftoff e-beam evaporation of 50 nm Ni/200 nm Au was performed. This processing produced parallel Ni/Au leads that fan out to contact pads and are electrically isolated unless crossed by an NW. The wafers were then electronically screened by varying V_{SD} from −1 to 1 V and measuring I_{SD}, and NW devices were revisited and the I_{SD} (V_{SD}) characteristics for varying V_G were determined. All measurements were taken with a HP 4156B semiconductor parameter analyser interfaced with a switchbox and a Cascade Microtech automated probestation with in-house created LabView software. Leads containing potential devices were then screened with field-emission scanning electron microscopy (FE-SEM) to determine the NW lengths and diameters and to eliminate multiple-NW devices. As in previous work [9], lengths were determined to the nearest 50 nm and diameters to the nearest 5 nm. All devices have linear I_{SD} (V_{SD}) dependences, with linear best-fit parameter $R^2 \geqslant 0.995$. In total 88 LA-CVD and 51 CVD devices are presented. Each growth was performed at least twice and devices were fabricated from each run. As seen previously for GaN NWs [9], growths with nominally identical growth variables produced NWs with statistically similar transport properties.

For variable-temperature measurements, the wafers were diced using a diamond scribe and dies were individually glued into 16-pin DIPs, wirebonded, and temperature-cycled in a Janis cryostat. An HP 4156B was used in manual mode for these measurements.

3. Results and discussion

Field-emission scanning electron microscope, transmission electron microscope (TEM), energy-dispersive spectroscopy (EDS), and micro-Raman characterizations of similarly fabricated LA-CVD In_2O_3 NWs have been previously described [12]. The NWs were determined to be single-crystal In_2O_3 growing in the [110] direction and were ∼4–8 μm long [12].

Scanning electron microscopy of the CVD samples revealed a large NW density on the growth substrates, figure 1(A). The NW lengths were found to range from 3–15 μm and the diameters varied from 10–100 nm. The NWs were not evenly dispersed, but predominantly located in scratched regions and near the edge. Interestingly, though the growth sequence is not yet known, the NWs appeared to emanate from In_2O_3 crystals, as seen previously for In_2O_3 nanobelts fabricated by thermal evaporation [26].

Transmission electron microscopy studies on CVD-fabricated NWs grown at 850 °C illustrate the presence of a Au nanoparticle at the tip of the In_2O_3 NW, figure 1(B),

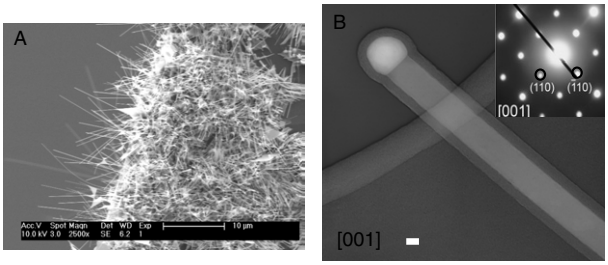

Figure 1. (A) FE-SEM image of CVD In_2O_3 NWs on the edge of the Si/SiO_2 growth substrate, where high NW densities exist; (B) TEM image of the tip of a CVD In_2O_3 NW with a ∼30 nm diameter. The gold catalyst is seen at the tip of the NW and the ∼10 nm amorphous coating the entire NW, including the Au tip, is readily apparent. The white bar represents 15 nm. The NW is lying on a graphite grid, one span of which is visible beneath the NW. The inset shows the diffraction pattern, indexed to [001] cubic In_2O_3 and, thus, a [110] growth direction.

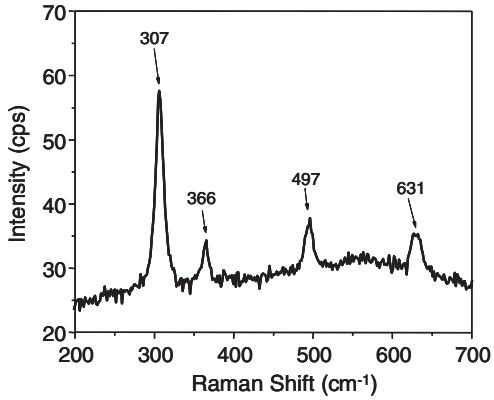

Figure 3. Micro-Raman spectra of a single In_2O_3 NW grown by CVD at 850 °C. The four E_g modes of cubic In_2O_3, 307, 366, 497, and 631 cm^{-1}, are highlighted.

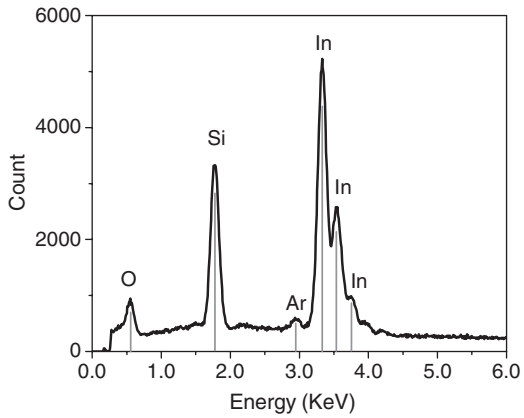

Figure 2. Energy-dispersive spectra of a single In_2O_3 NW grown by CVD at 850 °C on the Si/SiO_2 growth substrate. The In, O, Si, and Ar peaks are indexed.

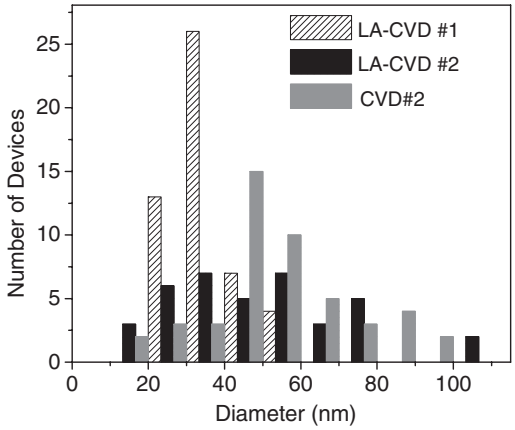

Figure 4. Diameter histogram of LA-CVD and CVD In_2O_3 NW devices. There are 50 LA-CVD samples and 47 CVD samples plotted. The average diameters of the NWs are given in table 1.

indicative of the VLS growth mechanism. The diffraction pattern has been indexed to the single crystal structure of [001] cubic In_2O_3, indicating the energetically preferable [110] NW growth direction. Most NWs were observed to be coated with an amorphous ∼10 nm In_2O_3 sheath. Because this sheath surrounds the NW and the growth catalyst we hypothesize that it is deposited during cooling. Further characterization with a high-resolution TEM is being undertaken.

Energy-dispersive spectroscopy on CVD-fabricated NWs grown at 850 °C indicates the sole presence of In and O in the NWs, figure 2. A Si peak is observed because the EDS was performed on samples on the Si/SiO_2 growth substrate. The slight presence of Ar is most likely due to its use as a carrier gas during NW growth. The room-temperature back-scattering micron-Raman spectrum for the CVD In_2O_3 NWs is exactly indexed to the four active E_g modes of cubic In_2O_3, 307, 366, 497, and 631 cm^{-1}, figure 3. These results are consistent with the previously published active modes for In_2O_3 crystalline powders [27–29].

The diameters of the NWs fabricated into devices are given in table 1. The NWs from LA-CVD #1 ranged from 20 to 55 nm, those from LA-CVD #2 ranged from 10 to 100 nm, and those from CVD #2 ranged from 10 to 95 nm, as illustrated in the histogram in figure 4. The greater uniformity of the LA-CVD sample diameters is most probably due to the use of Au catalyst particles: ∼30 nm Au nanoparticles were dispersed on the Si/SiO_2 for the LA-CVD growth, while the CVD fabrication relied on the high temperature to coalesce the Au thin-film on the Si/SiO_2 substrate into nanoparticles, resulting in a variation of catalyst particle sizes, reflected in the NW diameters. It is also seen that, as predicted by the VLS mechanism, higher growth temperatures produce NWs with greater diameters.

The n-type semiconducting behaviour of a representative In_2O_3 NW device from LA-CVD growths #1 and #2 and from CVD growth #2 is seen in the I_{SD} (V_{SD}) for varying V_{GD} dependences, figure 5. The FE-SEMs of the devices and the I_{SD} (V_{GD}) at $V_{SD} = 1$ V plots are inset in each panel. The linearity of the I_{SD} (V_{SD}) curve, indicative of ohmic metal–semiconductor contacts, is seen in figure 5. Although no Kelvin probe measurements could be made on a single NW due to insufficient NW lengths, the linear nature of the I_{SD} (V_{SD}) curves was preserved to 4 K for all four devices measured at variable temperature, consistent with negligible

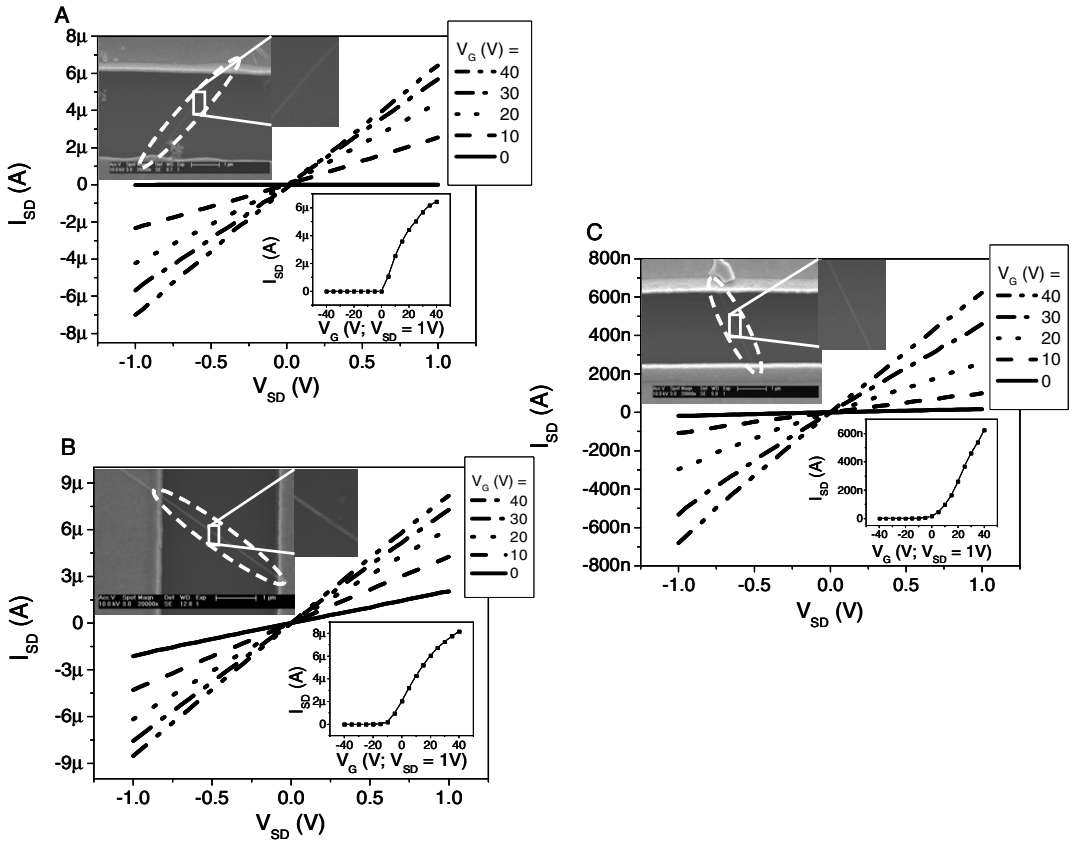

Figure 5. I_{SD} (V_{SD}) plot of a representative LA-CVD #1 (A), a representative LA-CVD #2 (B), and a representative CVD #2 (C) In_2O_3 NW device with the I_{SD} (V_{GD}) dependence inset. The NW device is circled in the inset FE-SEMs.

contact resistivities. Furthermore, the use of this contacting scheme on highly doped GaN NWs has previously been shown to produce ohmic contacts [30].

The I_{SD} (V_{SD}) and I_{SD} (V_{GD}) dependences in figures 5(A) and (B) are similar to those previously reported [12, 18], with an on/off ratio of $\sim 10^4$. In comparison, the on/off ratio of the CVD device is $\sim 10^3$, suggestive of a lower mobility. It should also be noted that, although all devices pinch off, the LA-CVD #1 NW turns off at $V_{GD} = 0$ V while the LA-CVD #2 and the CVD #2 samples do not turn off until a negative V_{GD} is reached. Most devices from all growths exhibited pinch-off. The transconductance was defined as the linear best-fit to the turned-on region of the I_{SD} (V_{GD}) at $V_{SD} = 1$ V curve. The mobility was then determined according to

$$\mu = \left(\frac{C}{L^2} V_{SD}\right)^{-1} \frac{\partial I_{SD}}{\partial V_{GD}}\bigg|_{V_{SD}=1}, \qquad (1)$$

where $C = \frac{2\pi\varepsilon\varepsilon_0 L}{\ln(4h/d)}$, L is the source–drain NW length, h is the oxide thickness, d is the NW diameter, and ε is 3.9 (SiO_2). The carrier concentration is then determined by

$$n = \frac{\sigma_{V_{GD}=0}}{e\mu}, \qquad (2)$$

with the conductance defined as the linear best-fit to the slope of the I_{SD} (V_{SD}) curve at $V_{GD} = 0$ V times the NW length divided by the NW cross-sectional area.

The mobilities and carrier concentrations were calculated for 50 LA-CVD devices from growth #1, 38 LA-CVD devices from growth #2, 4 CVD devices from growth #1, and 47 CVD devices from growth #2. Mobility versus carrier concentration plots for growth #1 and #2 are given in figures 6(A) and (B), respectively. For growth #1, the mobilities of the LA-CVD NWs vary from 30.9 to 359.3 $cm^2\ V^{-1}\ s^{-1}$, while those of CVD NWs lie between 2.6 and 42.6 $cm^2\ V^{-1}\ s^{-1}$. For growth #2, the mobilities of the LA-CVD NWs vary from 1.6 to 188.0 $cm^2\ V^{-1}\ s^{-1}$, while those of the CVD NWs lie between 0.1 and 45.8 $cm^2\ V^{-1}\ s^{-1}$. The average mobilities and carrier concentrations for the devices are given in table 1. It is seen that higher growth temperatures reduce the NW mobility but have little appreciable affect on the carrier concentration.

A t-test was performed on the two sample populations from growth #2 to determine if the transport properties of the samples were statistically different. The carrier concentrations are not different at the 95% confidence level; however, the mobilities are significantly different at the 99.9% confidence level ($t = 7.2$, $p = 2.3 \times 10^{-10}$).[7] These results are repeatable over multiple growth/fabrication runs.

In order to determine if the higher mobilities of the LA-CVD samples from growth #1 were due to their smaller

[7] In a t-test, the t-value is the ratio of the difference between the population means to the standard error of the mean, defined as $t = \frac{\bar{X}_T - \bar{X}_C}{\sqrt{\frac{\mathrm{var}_T}{n_T} + \frac{\mathrm{var}_C}{n_C}}}$. The p-value is the two-tailed probability computed using a t-distribution, with smaller values representing greater population separations.

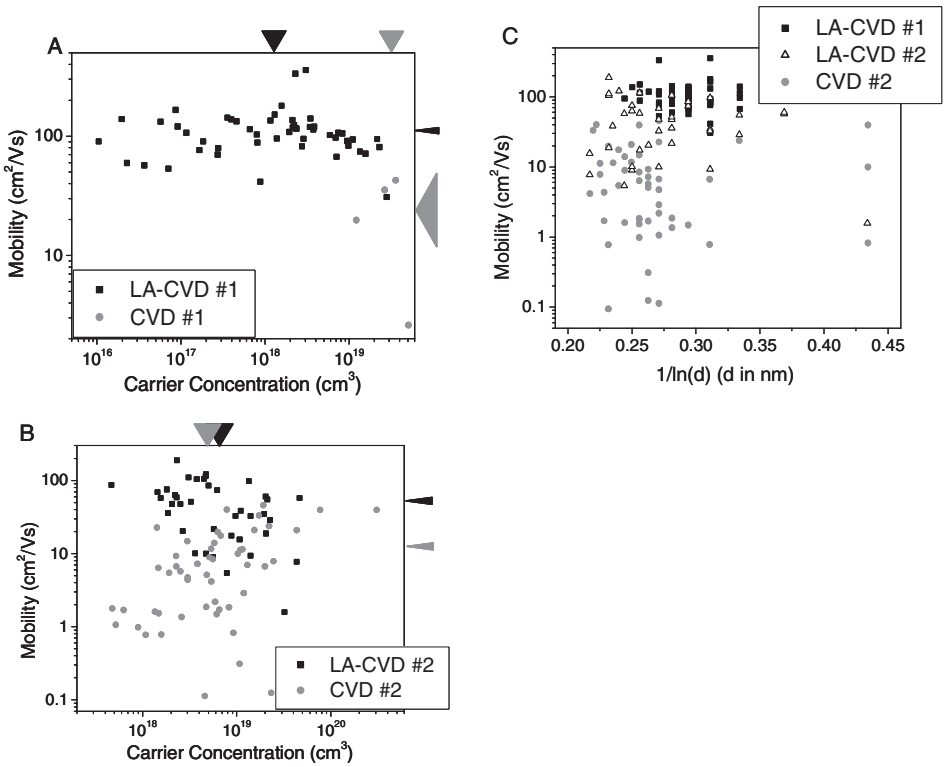

Figure 6. (A) Scatter plot of mobility versus carrier concentration for 50 LA-CVD #1 and 4 CVD #1 In_2O_3 NW devices. The arrows at the top and right of the plot lie at the average and their width corresponds to the standard error of the mean for LA-CVD #1 and to the standard deviation for CVD #1 (values given in table 1). (B) Scatter plot of mobility versus carrier concentration for 38 LA-CVD #2 and 47 CVD #2 In_2O_3 NW devices. The arrows at the top and right of the plot lie at the average and their width corresponds to the standard error of the mean (values given in table 1). (C) Plot of NW mobility versus $1/\ln(d)$, with d the NW diameter in nm, for LA-CVD #1, LA-CVD #2, and CVD #2 devices. No dependence is observed.

diameters compared with LA-CVD growth #2 and CVD growth #2, the mobility dependence on NW diameter was studied, figure 6(C). According to equation (1), the mobility for a specific material should be dependent on diameter according to $\mu \sim \frac{1}{\ln d}$. There is no appreciable dependence for either dataset in figure 6(C), with all linear best-fit coefficients $R^2 < 0.075$, indicating that the mobility variation is material rather than dimensionally dependent.

We next compare the LA-CVD and CVD In_2O_3 NWs to thin-film In_2O_3, which has also been grown with laser-ablation-assisted and unassisted CVD. Again assuming negligible metal–NW contact resistivities (ρ_C), the In_2O_3 resistivity values obtained in this work—averaging 6.1×10^{-6} Ω cm for LA-CVD #1 NWs, 1.9×10^{-6} Ω cm for LA-CVD #2 NWs, and 1.1×10^{-5} Ω cm for CVD #2 NWs—compare favourably to the literature values for thin-film In_2O_3—3.5×10^{-4} Ω cm for pulsed-laser-deposited In_2O_3 [31] and 2.2×10^{-3} Ω cm for ultrasonic-spray CVD-deposited In_2O_3 [32] and 2×10^{-4} Ω cm for thermally evaporated In_2O_3 [33]. As seen in thin films [31, 34] and as previously shown for LA-CVD NWs [18], growths with higher partial pressures of oxygen were also found to yield wires with lower carrier densities [35].

Four samples were then subjected to variable temperature measurements to elucidate the mechanisms underlying the higher quality of the LA-CVD NWs. Two NW devices from each growth system, one with a high mobility and one with a mid-to-low mobility, were selected and the temperature dependence of their mobilities is plotted in figure 7. The temperature dependence of the high-mobility samples, figures 7(A)–(C), shows the characteristic phonon scattering at temperatures >100 K and exhibits a mobility plateau at lower temperatures, in agreement with the literature for samples with high mobilities [36]. The temperature dependence of the mobility of the CVD NW sample with the low room-temperature mobility, ∼4 $cm^2\ V^{-1}\ s^{-1}$, parallels the literature for low-mobility samples, with a mobility peak at ∼150 K [36]. Below this temperature the mobility decreases for decreasing temperature, which would indicate dominant ionized impurity scattering.

4. Conclusion

We have demonstrated the successful synthesis of In_2O_3 NWs by unassisted CVD and have performed the first known comparison of LA and CVD growth techniques for NW synthesis. Our work shows that LA-CVD In_2O_3 NWs have significantly higher mobilities than their CVD counterparts. Furthermore, we have observed that In_2O_3 NW mobility increases with decreasing growth temperature. Since there is no appreciable change in yield with decreasing growth temperature for LA-CVD-fabricated NWs, whereas NW yield decreases dramatically with unassisted CVD, LA-CVD can

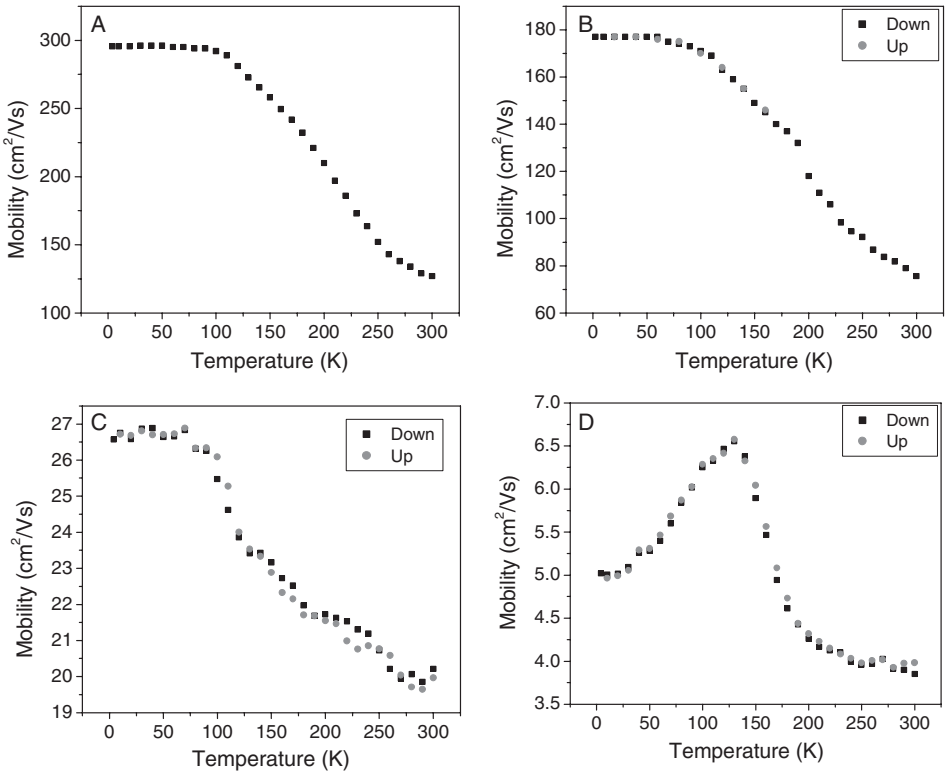

Figure 7. Variable-temperature dependence for four NW devices. Panels A and B are from LA-CVD In_2O_3 NWs with carrier concentrations of 2.2×10^{18} and 2.7×10^{17} cm^{-3}, respectively. Panels C and D are from CVD In_2O_3 NWs with carrier concentrations of 2.2×10^{19} and 1.5×10^{18} cm^{-3}, respectively.

access growth regimes for higher mobility material than unassisted CVD.

Acknowledgments

We would like to thank Dr James Klemic, Dr James Hyland, Mike Young, and David Routenberg for many helpful discussions, Dr Elena Cimpoiasu, Ryan Munden, and Aric Sanders for aiding with the measurement setup, and Dr Zhenting Jiang for help with the FE-SEM microscopy work. This work was partially supported by DARPA through AFOSR, ARO (DAAD19-01-1-0592), AFOSR (F49620-01-1-0358), NASA (NCC 2-1363), by a Department of Homeland Security graduate fellowship, and by an NSF graduate fellowship.

References

[1] Björk M T, Ohlsson B J, Sass T, Persson A I, Thelander C, Magnusson M H, Deppert K, Wallenberg L R and Samuelson L 2002 *Appl. Phys. Lett.* **80** 1058
[2] Björk M T, Ohlsson B J, Thelander C, Persson A O, Deppert K, Wallenberg L R and Samuelson L 2002 *Appl. Phys. Lett.* **81** 4458
[3] Gudiksen M S, Lauhon L J, Wang J, Smith D C and Lieber C M 2002 *Nature* **415** 617
[4] Huang Y, Duan X F and Lieber C M 2005 *Small* **1** 142
[5] Kuykendall T, Pauzauskie P, Lee S, Zhang Y, Goldberger J and Yang P 2003 *Nano Lett.* **3** 1063
[6] Poole P J, Lefebvre J and Fraser J 2003 *Appl. Phys. Lett.* **83** 2055
[7] Wu Z H, Mei X, Kim D, Blumin M, Ruda H E, Liu X L, Han J and Zhou C W 2003 *J. Mater. Res.* **18** 245
[8] Cheng G, Stern E, Tuner-Evans D and Reed M A 2005 *Appl. Phys. Lett.* **87** 253103
[9] Stern E *et al* 2005 *Nanotechnology* **16** 2941
[10] Rao C N R, Deepak F L, Gundiah G and Govindaraj A 2003 *Prog. Solid State Chem.* **31** 5
[11] Xia Y, Yang Y, Sun Y, Wu Y, Mayers B, Gates B, Yin Y, Kim F and Yan H 2003 *Adv. Mater.* **15** 353
[12] Li C, Zhang D, Han S, Liu X, Tang T and Zhou C 2003 *Adv. Mater.* **15** 143
[13] Hu J, Odom T W and Lieber C M 1999 *Acc. Chem. Res.* **32** 435
[14] Huang Y, Duan X, Cui Y and Lieber C M 2002 *Nano Lett.* **2** 101
[15] Zheng G, Lu W, Jin S and Lieber C M 2004 *Adv. Mater.* **16** 1890
[16] Stern E and Tutuc E 2006 unpublished data
[17] Stern E, Cheng G, Li C, Klemic J, Broomfield E, Turner-Evans D, Zhou C and Reed M A 2006 *J. Vac. Sci. Technol.* B **24** 231
[18] Lei B, Li C, Zhang D, Tang T and Zhou C 2004 *Appl. Phys.* A **79** 439
[19] Zhang D, Li C, Han S, Liu X, Tang T, Jin W and Zhou C 2003 *Appl. Phys.* A **77** 163
[20] Kim H W, Kim N H and Lee C 2005 *Appl. Phys.* A **81** 1919
[21] Li C, Zhang D, Liu X, Han S, Tang T, Han J and Zhou C 2003 *Appl. Phys. Lett.* **82** 1613
[22] Li C, Lei B, Zhang D, Liu X, Han S, Tang T, Rouhanizadeh M, Hsiai T and Zhou C 2003 *Appl. Phys. Lett.* **83** 4014
[23] Zhang D, Li C, Liu X, Han S, Tang T and Zhou C 2003 *Appl. Phys. Lett.* **83** 1845
[24] Zhang D, Zuqin L, Li C, Tang T, Liu X, Han S, Lei B and Zhou C 2004 *Nano Lett.* **4** 1919

[25] Tang T, Liu X, Li C, Lei B, Zhang D, Rouhanizadeh M, Hsiai T and Zhou C 2005 *Appl. Phys. Lett.* **86** 103903
[26] Kong X Y and Wang Z L 2003 *Solid State Commun.* **128** 1
[27] Wang J X *et al* 2005 *J. Cryst. Growth* **284** 73
[28] Rong Q J, Osaka A, Nanba T, Takada J and Miura Y 1992 *J. Mater. Sci.* **27** 3793
[29] Korotcenkov G, Brinzari V, Ivanov M, Cerneavschi A, Rodriguez J, Cirera A, Cornet A and Morante J 2005 *Thin Solid Films* **479** 38
[30] Stern E, Cheng G, Young M A and Reed M A 2006 *Appl. Phys. Lett.* **88** 053106
[31] Adurodija F O, Semple L and Brüning R 2005 *Thin Solid Films* **492** 153
[32] Girtan M 2004 *Surf. Coat. Technol.* **184** 219
[33] Pan C A and Ma T P 1980 *Appl. Phys. Lett.* **37** 163
[34] de Wit J H W 1973 *J. Solid State Chem.* **8** 142
[35] Stern E, Cheng G and Guthrie S 2006 unpublished data
[36] Weiher R L 1962 *J. Appl. Phys.* **33** 2834